Journal of Dental Research
2016, Vol. 95(7) 776–783

DOI: 10.1177/0022034516634664
jdr.sagepub.com

Identification of Stem Cells in the Secretory Complex of Salivary Glands

M. Kwak[1], N. Alston[1], and S. Ghazizadeh[1]

Abstract

Salivary glands have an essential secretory function for maintaining oral and overall health. The epithelial compartment of the gland is composed of several highly specialized cell types that cooperate to secrete and deliver saliva to the oral cavity. The mouse submandibular gland has been used as a model for major salivary glands in human. The secretory complex in this model is composed of 2 secretory compartments, including acini and granular ducts connected by intercalated ducts. Contractile myoepithelial cells surround the secretory complex to facilitate salivary flow. Whether differentiated cells in the secretory complex are maintained by self-duplication or contribution from stem cells has remained an open question. Here, in analyzing the expression of basal cytokeratin (K) 14 in the secretory complex, we discovered a subset of $K14^+$ ductal cells in the intercalated ducts of the adult gland. These cells are distinct from the K14-expressing basal/myoepithelial cells, proliferate at a significantly higher rate than any other epithelial cell type in the gland, and reside in a spatially defined domain within the intercalated duct. Using inducible genetic lineage tracing, we show that $K14^+$ ductal cells represent a long-lived yet cycling population of stem cells that are established during development and contribute to the formation and maintenance of the granular ducts throughout life. Our data provide direct evidence for the existence of stem cells contributing to homeostasis of salivary glands, as well as new insights into glandular pathobiology.

Keywords: submandibular gland, progenitors, keratin-14, development, cell lineage, homeostasis

Introduction

Major salivary glands contribute to secretion of 90% of saliva and include 3 pairs of glandular organs: parotid, submandibular, and sublingual. A typical gland is a glandular epithelium composed of acini, ducts, and myoepithelial cells surrounded by a stromal matrix. Acini, the secretory end piece, secrete the saliva into the lumen of a contiguous ductal network of the intercalated, granular/striated, and excretory ducts, which modify the primary saliva before it reaches the oral cavity (Amano et al. 2012). Nerve-mediated contraction of myoepithelial cells that surround the secretory complex facilitates release and flow of saliva (Emmelin et al. 1968). The rodent submandibular gland (SMG) has been widely used as a model to study salivary gland development (Melnick and Jaskoll 2000). The mouse SMG begins to develop from the oral epithelium during embryogenesis and continues postnatally with adult-type acini and the granular ducts (GDs), a specialized segment of striated duct most prominent in rodents, emerging at puberty (Gresik 1994; Tucker 2007). A sexual dimorphism in differentiation of GD cells results in morphologic sex differences, mainly in the proportion of GDs, which occupy 45% to 65% of the gland in males but only 30% to 36% in females (Chai et al. 1993; Gresik 1994). In adult mice, the secretory complex of SMG is composed of acini and GDs, 2 highly specialized secretory compartments separated by intercalated ducts and surrounded by myoepithelial cells (Denny et al. 1997; Amano et al. 2012).

The adult salivary gland renews relatively slowly, at an average rate of 2 to 4 mo in rodents (Schwartz-Arad et al. 1988; Zajicek et al. 1989). Like many epithelial tissues, salivary gland homeostasis is thought to rely on stem cells (Denny et al. 1997; Pringle et al. 2013). Tissue stem cells are defined as relatively undifferentiated cells that have the capacity to self-renew and generate progenies that are fated to differentiate (Lajtha 1979). In the adult SMG, cells in the intercalated ducts and the basal layer of excretory ducts retain a relatively undifferentiated morphology and divide more frequently when compared with other parenchymal cell types (Zajicek et al. 1985; Schwartz-Arad et al. 1988; Denny, Chai, et al. 1993). Our recent genetic studies have revealed a progenitor-progeny relationship between $K14^+$ basal cells and the terminally differentiated $K19^+$ luminal cells in the excretory ducts (Kwak and Ghazizadeh 2015). However, contrary to the excretory ducts where luminal cells are postmitotic, all well-differentiated cell lineages in the secretory complex, including acinar, GD, and

[1]Department of Oral Biology and Pathology, Stony Brook University, Stony Brook, NY, USA

A supplemental appendix to this article is published electronically only at http://jdr.sagepub.com/supplemental.

Corresponding Author:
S. Ghazizadeh, Department of Oral Biology and Pathology, Stony Brook University, New York, NY 11794-8702, USA.
Email: soosan.ghazizadeh@stonybrook.edu

myoepithelial cells, remain mitotically active and may contribute to cell renewal in the adult gland (Zajicek et al. 1985; Denny, Denny, et al. 1993; Aure, Konieczny, et al. 2015; Kwak and Ghazizadeh 2015). To date, there has been no direct evidence for stem cell contribution to various cell lineages in the secretory complex, and a recent genetic lineage tracing of acinar cells in mice identified self-duplication of differentiated acinar cells as the predominant mechanism for expansion and maintenance of the acini after birth (Aure, Arany, et al. 2015; Aure, Konieczny, et al. 2015).

Here, while analyzing dynamics of K14 expression in the secretory complex during postnatal SMG development, we discovered that a subset of $K14^+$ ductal progenitors in the developing gland persists in the intercalated ducts of the adult gland. Using an inducible genetic lineage-tracing approach, we show that these cells represent tissue stem cells that contribute to the development and homeostasis of GDs throughout life.

Materials and Methods

Animals

Transgenic K14-rtTA (stock 008099), tetO-H2BGFP (stock 005104), tetO-Cre (stock 006234), and RosaYFP (stock 006148) were purchased from Jackson Laboratory (Bar Harbor, ME, USA) and crossed to generate bitransgenic mice (K14rtTA:tetOH2BGFP) or triple-transgenic mice (K14rtTA:tetOCre:RosaYFP). Label was induced either by doxycycline (Dox)–containing food (1 g/kg of pellets; BioServ, Flemington, NJ, USA) or by intraperitoneal injection (1 mg/20 g of weight). Animals were housed under standard conditions, and all animal experiments were performed in accordance with institutional guidelines set forth by the State University of New York.

Antibodies and Histologic Analysis

The primary antibodies are listed in the Appendix, and immunofluorescent analysis has been described (Kwak and Ghazizadeh 2015). For coimmunostaining, when antibodies to cell-specific markers were made in the same species, staining was done sequentially. Sections were examined with a Nikon E800 fluorescent microscope, and images were captured with NIS-Elements (Nikon Instrument Inc., Melville, NY, USA). For quantification of YFP-labeled clusters (≥5 cells), tissue sections were costained for YFP and integrin-α6 (to mark all parenchymal cells), and the number of YFP-labeled clusters in 25 randomized 100× images per time point were counted. The average area (size) of YFP^+ clusters per image was quantified with Image J.

Analysis of Cell Proliferation

To determine the BrdU-labeling index in various compartments, adult mice (8 wk of age) were injected with BrdU (50 μg/g of body weight; Sigma, St. Louis, MO, USA), and 4 h later, SMGs were removed and costained for BrdU and cell-specific markers as described previously (Kwak and Ghazizadeh 2015). The proportion of BrdU-positive nuclei to total number of nuclei in each compartment was determined by analysis of a minimum of 24 images (400×) per compartment per mouse. To accurately access the BrdU-labeling index of $K14^+$ intercalated duct cells, the BrdU-labeling index for K14-expressing cells (counting a total of 3,836 nuclei) and that of smooth muscle actin (SMA)–expressing cells (counting a total of 2,700 nuclei) in the secretory complex were quantified; then, the BrdU-labeling index of myoepithelial cells was deducted from that of K14-expressing cells.

Statistical Analyses

Differences among means were evaluated either by Student's 2-tailed unpaired *t* test (when 2 groups were compared) or by 1-way analysis of variance followed by Tukey's honestly significant difference post hoc test (when several groups were compared). SPW12 (Systat Software Inc., San Jose, CA, USA) statistical software was used. Values with $P < 0.05$ were accepted as significant.

Results

K14 Marks a Subset of Intercalated Ductal Cells in the Adult Mouse SMG

Although K14 is broadly expressed in the developing ducts during postnatal development (Nelson et al. 2013; Kwak and Ghazizadeh 2015), its expression appears to be restricted to the basal excretory duct and myoepithelial cells in the adult salivary glands (Ogawa et al. 2000; Ihrler et al. 2002). To gain insights into the temporal and spatial expression pattern of K14 in salivary ducts, K14 expressions in mouse SMG at 2, 4, 6, and 8 wk of age were analyzed by immunostaining. Since the secretory complex is surrounded by myoepithelial cells, tissue sections were costained with antibodies to K14 and SMA to distinguish $K14^+SMA^-$ cells from $K14^+SMA^+$ myoepithelial cells. This analysis revealed a progressive decline in the proportion of $K14^+SMA^-$ cells, from 19.6% ± 1.2% at 2 wk of age to 5% ± 0.3% at 6 wk of age (Fig. 1A, B; Appendix Fig. 1), coinciding with differentiation and expansion of the GDs (Redman and Sreebny 1970; Gresik 1994; Tucker 2007). However, a subset of $K14^+SMA^-$ cells localized to the intercalated duct was detected in the mature gland (6 to 8 wk of age; Fig. 1A–C). Cross sections of intercalated ducts showed that, contrary to myoepithelial cells that surrounded the duct, $K14^+SMA^-$ cells occupied a luminal (ductal) position (Fig. 1C, lower panels). Given the age- and sex-dependent changes in the rate and mechanism of cell renewal in the mouse SMG (Chai et al. 1993; Denny et al. 1997), we examined the frequency and distribution of $K14^+SMA^-$ cells in 1-y-old male and female mice. Remarkably, $K14^+SMA^-$ cells were located at the same region of SMG in these mice, although their frequency was significantly higher in females (Fig. 1D, E).

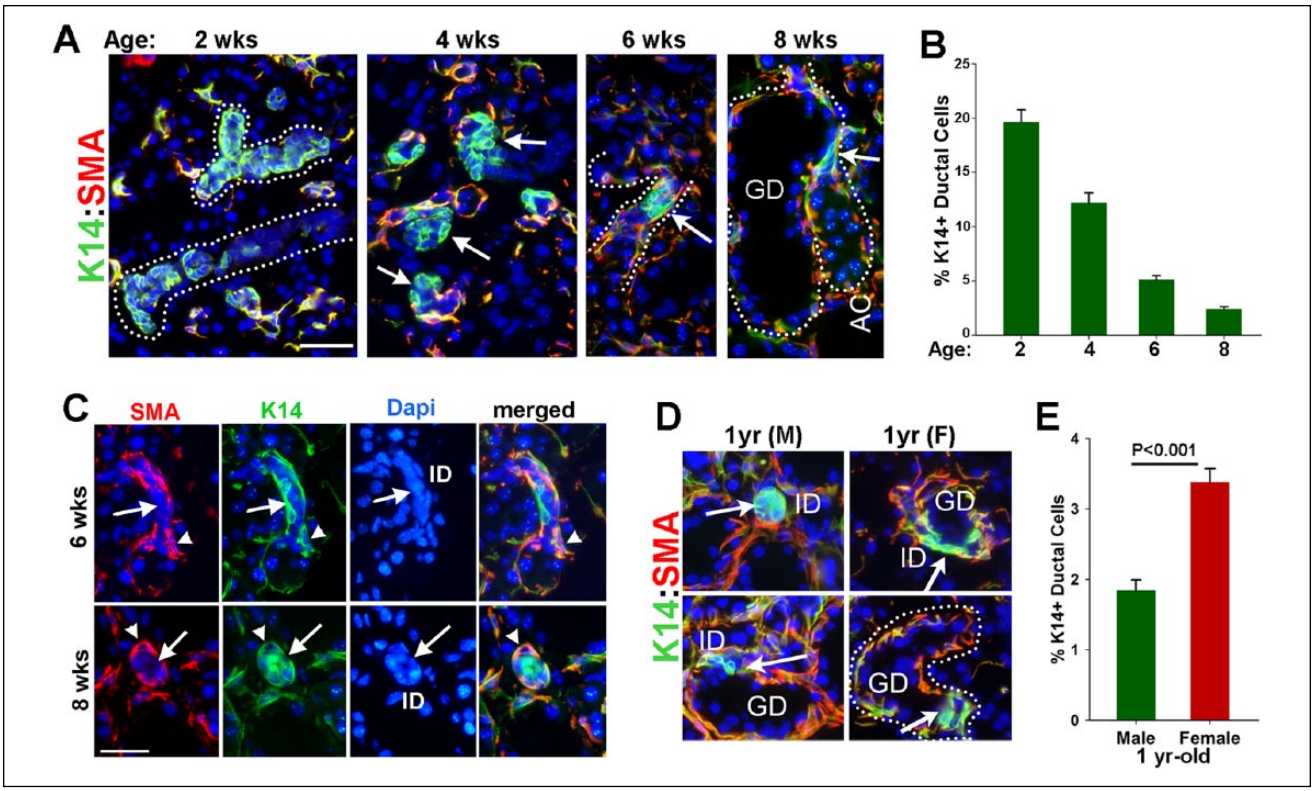

Figure 1. Identification of K14-expressing ductal cells in the secretory complex. (**A**) Immunofluorescent images of sections of submandibular gland obtained from male mice and coimmunostained with antibodies to K14 (green) and smooth muscle actin (SMA; red). Sections were counterstained with dapi (blue nuclear staining). (**B**) The percentage of $K14^{+}SMA^{-}$ cells to the total number of $dapi^{+}$ nuclei in the gland of male mice at different age is shown. Values are expressed as mean ± SEM with cell counts obtained from a minimum of 25 images (400×) per 2 mice per age. $P < 0.001$ by analysis of variance with Tukey's post hoc test. (**C**) Immunofluorescent images of intercalated ducts in the mature gland stained as described in panel A showing only a partial overlap between K14 and SMA markers in the ID. (**D**) Immunofluorescent images of submandibular gland sections obtained from 1-y-old male (M) and female (F) mice and costained for K14 and SMA. For all panels, arrows point to $K14^{+}SMA^{-}$ ductal cells, and arrowheads note myoepithelial cells. (**E**) Percentage of $K14^{+}SMA^{-}$ cells in 1-y-old male and female mice was measured as described in panel B with 50 images from 2 mice per sex. Scale bars: 50 µm. AC, acini; ID, intercalated duct; GD, granular duct.

To confirm these findings, we used an inducible genetic labeling system to selectively mark $K14^{+}$ cells and map their location more precisely in the adult SMG. Bitransgenic K14rtTA:tetOH2BGFP mice have been used to selectively label $K14^{+}$ cells with nuclear green fluorescent protein (GFP) during SMG development (Kwak and Ghazizadeh 2015). In these mice, histone H2B-GFP expression is driven by K14 promoter and regulated by tetracycline-responsive elements (Waghmare et al. 2008). To induce label during adulthood, mice were fed a Dox diet from 6 to 12 wk of age (Fig. 2A). SMGs were biopsied, and the location of cells with nuclear GFP were mapped in relation to various compartments of the secretory complex through cell-specific markers, including Aqp5 (acini), cKit (intercalated ducts), and K19 (GDs; Fig. 2B). Labeled cells were either organized into small clusters localized to the intercalated ducts (Kit^{+}) or distributed as singly labeled cells (Fig. 2B, C; Appendix Fig. 2). Immunofluorescent analysis showed that all cells with high GFP intensity (GFP^{hi}) expressed K14 (Fig. 2C); however, only a subset of GFP^{hi} cells expressed SMA (Fig. 2D). Interestingly, the labeled clusters included both $K14^{+}$ and $K14^{-}$ cells, although the GFP intensity in the latter was markedly lower (Fig. 2C, D). Overall, these data verified the presence of 2 distinct populations of $K14^{+}$ cells in the secretory complex, including myoepithelial cells and a subset of intercalated duct cells (Fig. 2E).

$K14^{+}$ Intercalated Ductal Cells Represent an Actively Cycling Cell Population

To assess the replicative behavior of $K14^{+}$ ductal cells, we subjected the K14rtTA:tetOH2BGFP mice to a short pulse-chase experiment. In this system, during the chase period, H2BGFP induced by pulse labeling remains incorporated into chromatin due its high stability, unless the cell divides. On each cell division, H2BGFP is diluted by half, allowing evaluation of cycling behavior of the labeled population (Waghmare et al. 2008). Bitransgenic mice were fed with Dox from 4 to 6 wk of age, and H2BGFP-labeled cells were analyzed after a 2-wk period of chase at 8 wk of age (Fig. 3A). Immediately following pulse labeling, H2BGFP was restricted to the $K14^{+}$ ductal and myoepithelial cells (Fig. 3B, upper panels). After 2 wk of chase,

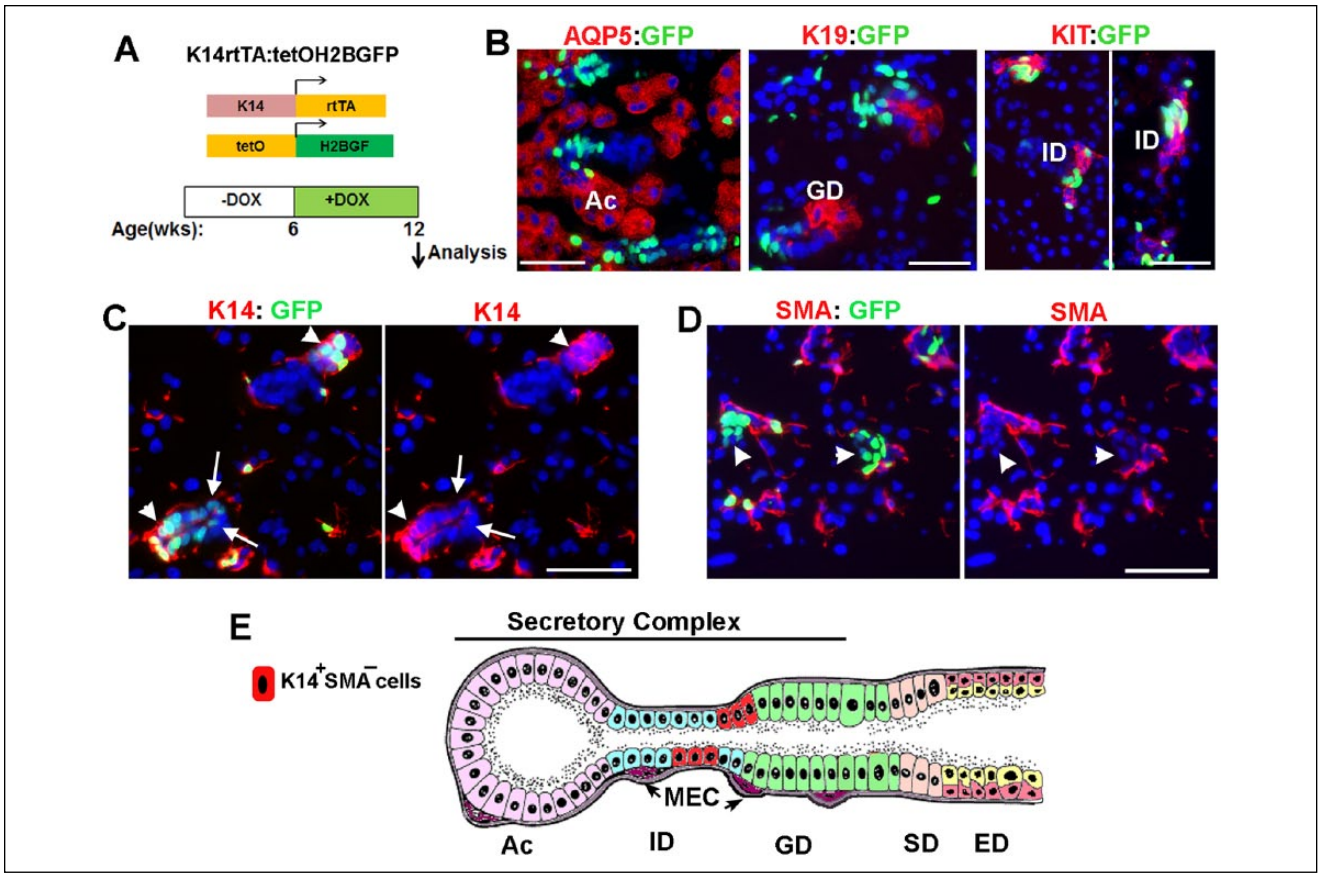

Figure 2. K14 gene driver targets 2 distinct cell populations in the secretory complex of adult submandibular gland (SMG). (**A**) Strategy used to label K14-expressing cells with nuclear GFP in adult mice. (**B**) Representative fluorescent images of GFP-labeled SMG at 12 wk of age stained with Aqp5, K19, and Kit (in red) to map the location of nuclear GFP (green) in the secretory complex. (**C**, **D**) Immunofluorescent images of labeled SMG stained for K14 or smooth muscle actin (SMA; red). Arrowheads point to the GFP-labeled ductal cell clusters. Arrows note the GFP^+K14^- cells. Sections were counterstained with dapi (blue). Scale bars: 50 µm. (**E**) A schematic representation of the SMG showing the location of $K14^+SMA^-$ ductal cells in the secretory complex. AC, acini; Dox, doxycycline; ED, excretory duct; GD, granular duct; ID, intercalated duct; MEC, myoepithelial cells; SD, striated duct.

H2BGFP (nuclear green fluorescence) was barely detectable in the $K14^+$ ductal cells and appeared in the adjacent $K14^-$ cells that included $K19^+$ ductal cells (Fig. 3B, lower panels, arrowheads). Contrary to the $K14^+$ ductal cells, labeled myoepithelial cells retained high levels of H2BGFP during the chase period (Fig. 3B). The relatively rapid loss of H2BGFP from $K14^+$ ductal cells was consistent with the behavior of an actively cycling cell population.

To verify these findings, we used BrdU labeling to assess the relative proliferation rate of $K14^+$ ductal cells in comparison with other epithelial cell populations. A single dose of BrdU was administered at 8 wk of age to label cells in the S phase of the cell cycle, and the frequency of DNA replication in various compartments was determined. BrdU-labeling index for $K14^+$ ductal cells was measured at 9% ± 1.9%, several folds higher than any other compartment in the gland (Fig. 3C). Taken together, both H2BGFP dilution assay and BrdU-labeling index identified $K14^+$ duct cells as an actively cycling cell population in the adult SMG.

$K14^+$ Intercalated Ductal Cells are a Self-renewing Cell Population Contributing to the Formation and Maintenance of GDs

To assess the potency and fate of $K14^+$ ductal cells, we employed an inducible lineage-tracing strategy using K14 promoter with Cre reporter RosaYFP mice, in which a floxed stop codon that exists between the ubiquitously expressed Rosa26 promoter and YFP gene is permanently excised upon Cre activation, allowing for fate mapping of the originally labeled $K14^+$ cells and their descendants over a long period of time (Mao et al. 2001). RosaYFP mice were crossed with K14rtTA:tetOCre mice, and a single dose of Dox was administered at 6 wk of age to activate K14-Cre (Fig. 4A). Analysis of SMGs 4 d later confirmed selective labeling of $K14^+$ cells, including ductal and myoepithelial cells (Fig. 4B). Six weeks later, immunofluorescent analysis of tissue sections showed clusters of RosaYFP lineage-traced cells at the distal region of GDs ($K19^+$) that extended into the intercalated duct–GD junction

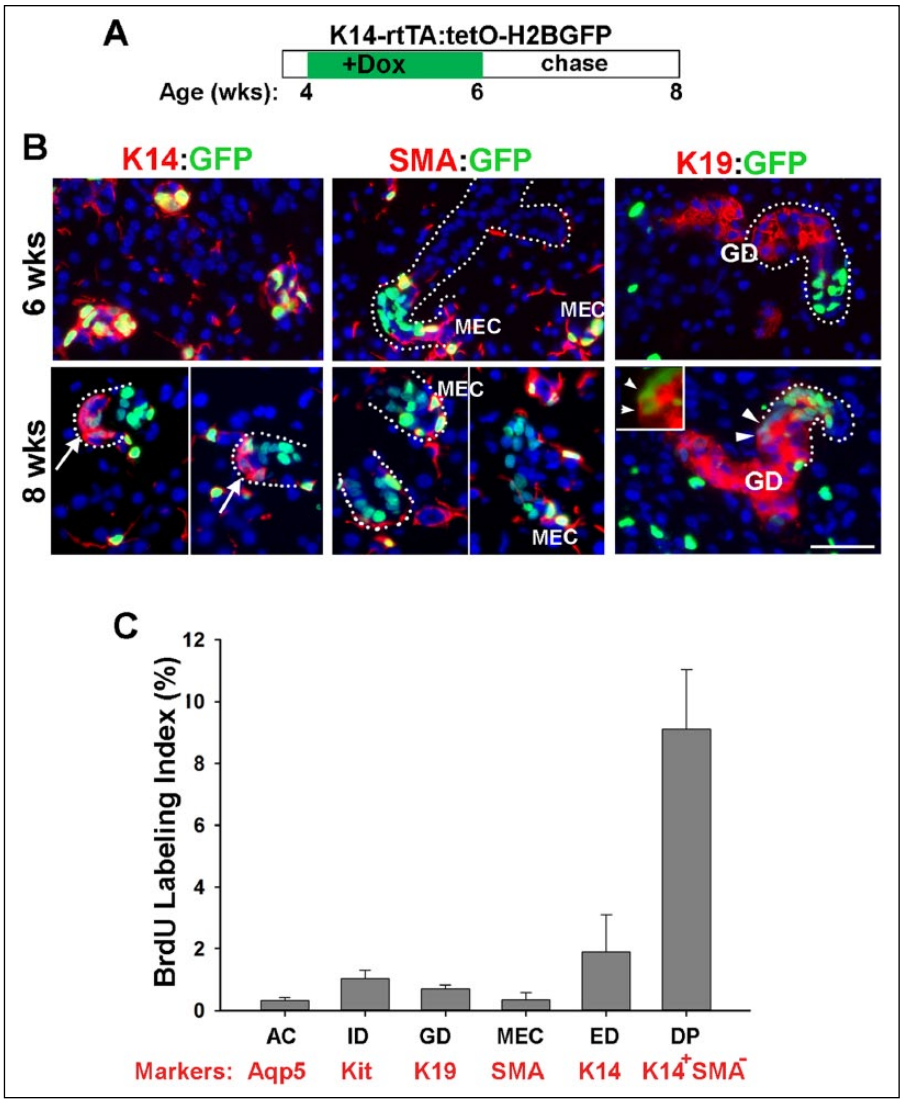

Figure 3. K14$^+$ ductal cells are an actively cycling cell population in the adult submandibular gland (SMG). (**A**) Pulse labeling and chase strategy. Doxycycline (Dox) diet was administered for 2 wk, and SMGs were analyzed either immediately after pulse labeling (6 wk) or after a 2-wk chase period (8 wk). (**B**) Representative images of H2BGFP-labeled SMGs stained for K14, smooth muscle actin (SMA), or K19 (in red). Arrows point to the low intensity of nuclear GFP in K14$^+$ ductal cells after the chase period. Arrowheads note the location of K19$^+$ cells with dim nuclear green fluorescence. Inset is a higher magnification of K19$^+$GFP$^+$ cells. Nuclear blue staining is dapi. Scale bars: 50 µm. (**C**) BrdU-labeling index of acini (AC), intercalated ducts (ID), granular ducts (GD), myoepithelial cells (MEC), excretory ducts (ED), and K14$^+$ intercalated ductal cells (DP) in 8-wk-old male mice after a 4-h BrdU pulse. SMG sections were coimmunostained with antibodies to BrdU and to cell-specific markers indicated at the bottom of the graph. Values are expressed as mean ± SEM in each compartment with a minimum of 24 images (400×) per compartment per mouse (n = 2 per age). $P < 0.001$ based on analysis of variance, followed by Tukey's post hoc test.

where K14$^+$ ductal cells reside (Fig. 4C). Neither the Kit$^+$ intercalated duct cells nor the acini were labeled (Fig. 4C). These results indicated that the descendants of the initially labeled K14$^+$ cells expanded unidirectionally into the GDs.

To determine the contribution of K14$^+$ ductal cells to postnatal SMG development when K14 is broadly expressed in presumptive intercalated ducts (Fig. 1A), we administered Dox to newborn mice during the first week of life (Fig. 4D, Appendix Fig. 3). Analysis of labeled SMGs 4 wk later revealed larger YFP$^+$ clusters; however, similar to the adult gland, the RosaYFP lineage-traced cells were restricted to the GDs (Fig. 4E, F; Appendix Fig. 3). Immunostaining for K14 verified the presence of YFP-labeled K14$^+$ cells in the intercalated ducts that were contiguous with the YFP$^+$GDs (Fig. 4F, arrows). Although Cre activation could result in labeling of myoepithelial cells (K14$^+$SMA$^+$), most SMA$^+$ cells, including those surrounding the labeled clusters, were not marked with YFP (Fig. 4F, arrowheads).

Tissue stem cells are established during development and can be distinguished from transit progenitor cells by their ability to undergo long-term self-renewal (Blanpain and Fuchs 2014). To determine whether the K14$^+$ ductal cells represent a long-lived stem cell population, we extended the chase period to 28 wk. Analysis of SMG after this long period of chase showed persistence of the initially labeled K14$^+$ ductal cells and further expansion of RosaYFP lineage-traced cells in the GDs but not into the adjacent Kit$^+$ region of the intercalated ducts (Fig. 4G, Appendix Fig. 3). A quantitative analysis of YFP-labeled clusters at 4 and 28 wk of chase verified the stability and continued expansion of a large fraction (~70%) of labeled clusters (Fig. 4H–J).

Overall, the long-term persistence of K14$^+$ ductal cells and their expansive progeny are consistent with the establishment of a lineage-restricted stem cell population in the intercalated duct contributing to the formation and maintenance of the GDs during postnatal development and homeostatic turnover.

Discussion

In the present study, we report identification of a long-lived yet actively cycling population of stem cells in the intercalated duct that is established during postnatal development and that continually replenishes the differentiated cells in the GD during homeostasis. Compartmentalization of stem cells and their differentiated progeny has also been shown in the excretory duct where cells in the basal layer maintain the luminal (suprabasal) cells (Kwak and Ghazizadeh 2015). Therefore, there are at least 2 distinct populations of stem cells—one in the excretory duct and another in the intercalated duct—maintaining cell renewal in the

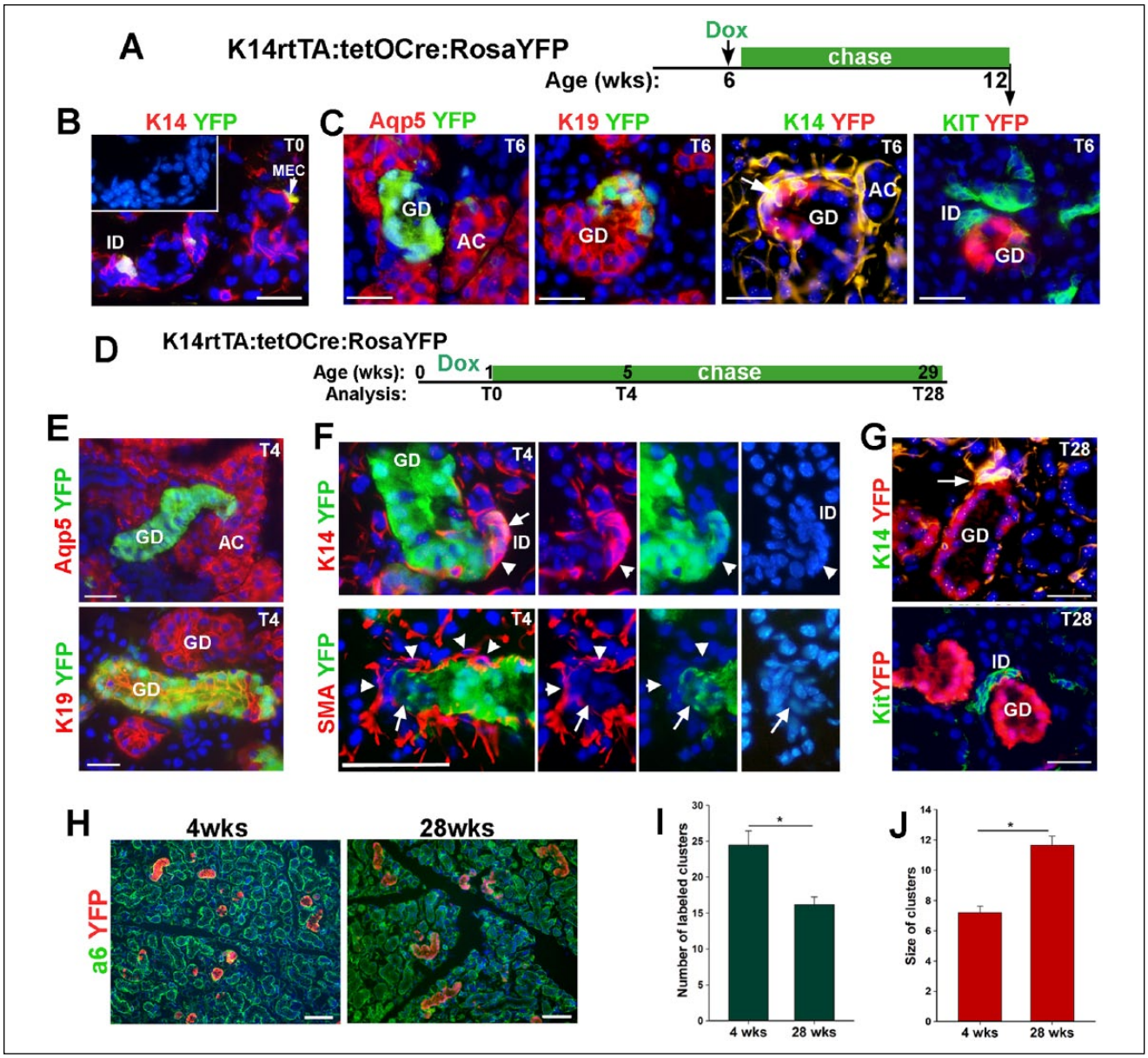

Figure 4. K14 marks a lineage-restricted stem cell population contributing to the formation and maintenance of granular ducts. (**A**) K14rtTA/tetOCre mice were crossed with RosaYFP, and Cre was induced in 6-wk-old trigenic mice by a single injection of 0.25 mg of doxycycline (Dox). Submandibular glands (SMGs) were analyzed either at 3 d (T0) or 6 wk (T6) of chase. (**B**) Colocalization of YFP (green) and K14 (red) in SMG at T0. The inset is dapi staining to show the ductal position of the labeled cell, and the arrowhead points to a labeled myoepithelial cell (MEC). (**C**) Images of SMG after 6 wk of chase stained for YFP, with lineage markers indicated at the top of each panel. Arrow in panel C points to YFP-labeled $K14^+$ cells. Blue nuclear staining is dapi. Images are from male transgenic mice and representative of both sexes (n = 2 per sex). (**D**) Labeling strategy for lineage tracing during postnatal development. (**E**, **F**) Representative images of labeled SMG from females at 5 wk of age (n = 3 per sex) stained with antibodies to YFP (green) and cell lineage markers (in red). For K14 and smooth muscle actin (SMA), individual staining is included to show the relative position of labeled $K14^+$ cells (arrows) and myoepithelial cells. Arrowheads point to myoepithelial cells that do not express YFP. (**G**) Images of SMG after 28 wk of chase stained with antibodies to YFP (red) and either K14 or Kit (green). Arrow points to YFP^+ stem cells (orange). Scale bars (B–G): 50 µm. (**H**) Representative images of SMG after 4 and 28 wk of chase stained for YFP (red) and integrin-a6 (green) to show stability of labeled clusters. Scale bars: 100 µm. (**I**, **J**) Quantification of YFP-labeled clusters comparing the number (I) and the size (J) of the labeled clusters after 4 and 28 wk of chase. Values are expressed as mean ± SEM with 25 images (100×) per group. *P < 0.001. AC, acini; GD, granular duct; ID, intercalated duct.

salivary gland duct system. The prevailing model of cell renewal in the salivary gland proposes that a population of primitive stem cells in the excretory duct supplies the distal progenitors in the intercalated ducts that eventually replenish the more differentiated cell types in the secretory complex (Pringle et al. 2013). Although our studies demonstrate a role for stem cells in maintaining salivary gland homeostasis, our lineage-tracing studies do not support a hierarchical model. The

existence of 2 distinct stem cell populations in the salivary ducts is consistent with other complex epithelial tissues that are maintained by multiple spatially and temporally restricted stem cell populations (Blanpain and Fuchs 2014; Hogan et al. 2014).

Although K14 is a well-established marker of basal/myoepithelial cells in the salivary glands, expression of basal-type keratins in the intercalated ductal cells has not been previously reported (Ogawa et al. 2000; Ihrler et al. 2004). Without costaining for K14 and SMA, it is difficult to distinguish a small subset of intercalated duct cells from the surrounding myoepithelial cells. Our analysis revealed a significant difference in the replicative behavior of these 2 cell populations. Myoepithelial cells are mostly quiescent, while $K14^+$ ductal cells cycle frequently. Recent studies in mammary gland have identified a bipotent basal/myoepithelial stem cell population giving rise to the luminal progenitors that contribute to the duct maintenance (Rios et al. 2014). Although a clear lineal relationship between $K14^+$ ductal cells and myoepithelial cells in the SMG could not be established in our mouse model, the presence of nonlabeled myoepithelial cells surrounding YFP-labeled clusters or nonlabeled GDs encircled by YFP-labeled myoepithelial cells after a long period of chase (Appendix Fig. 3C, D) suggests that myoepithelial and ductal cells are maintained independently.

The unidirectional expansion of labeled cells from intercalated ducts to GDs revealed by our studies is consistent with the classical ^{3}H-thymidine-tracking studies that showed streaming of the cells from the stem or trunk portion of the intercalated duct to the GD (Chai et al. 1993; Denny et al. 1997). These studies also noted a significantly higher labeling index for a subset of cells near the intercalated-GD junction. This population was described as an intermediate cell between a modestly replicating stem cell in the intercalated duct and the slowly dividing differentiated GD cells (Chai et al. 1993; Denny et al. 1997). Our studies, however, indicate that the actively cycling cells in the intercalated ducts are indeed long-lived stem cells.

A recent lineage-tracing study in mice with an acinar-specific gene driver concluded that self-duplication of acinar cells is not only responsible for acinar renewal during homeostasis but also contributes to acinar expansion during postnatal development and regeneration (Aure, Konieczny, et al. 2015). The lack of contribution from $K14^+$ stem cells to acini during postnatal development supports this conclusion. However, acinar differentiation in the parotid gland and SMG continues postnatally (Redman 2008), and the new acini and their associated intercalated ducts are added at a rate requiring input from progenitors (Denny et al. 1990; Denny et al. 1997). Given the heterogeneity of intercalated ductal cells, a second population of progenitor/stem cells may contribute to acinar formation during rapid growth. The partitioning of Kit^+ and $K14^+$ markers in the intercalated ducts and the lack of contribution from $K14^+$ stem cells to the Kit^+ cells indicate that the Kit^+ cell lineage is maintained independently. Whether Kit^+ ductal cells contribute to acinar formation during early stages of postnatal development awaits further investigation.

In conclusion, we have identified an actively cycling stem cell population in the secretory complex that may have implications in radiation-induced damage as well as neoplasia. Deciphering the signaling pathways regulating the self-renewal and fate determination of this stem cell population could result in strategies for treating disorders of this vital and complex organ.

Author Contributions

M. Kwak, contributed to conception, design, data acquisition, analysis, and interpretation, drafted the manuscript; N. Alston, contributed to data acquisition, critically revised the manuscript; S. Ghazizadeh, contributed to conception, design, and data analysis, drafted and critically revised the manuscript. All authors gave final approval and agree to be accountable for all aspects of the work.

Acknowledgments

The authors thank Laurie Levine for technical assistance with mouse colonies. This work was supported by the National Institute of Dental and Craniofacial Research of the National Institutes of Health (R21DE022959 to S.G.). The authors declare no potential conflicts of interest with respect to the authorship and/or publication of this article.

References

Amano O, Mizobe K, Bando Y, Sakiyama K. 2012. Anatomy and histology of rodent and human major salivary glands: overview of the japan salivary gland society-sponsored workshop. Acta Histochem Cytochem. 45(5):241–250.

Aure MH, Arany S, Ovitt CE. 2015. Salivary glands: stem cells, self-duplication, or both? J Dent Res. 94(11):1502–1507.

Aure MH, Konieczny SF, Ovitt CE. 2015. Salivary gland homeostasis is maintained through acinar cell self-duplication. Dev Cell. 33(2):231–237.

Blanpain C, Fuchs E. 2014. Stem cell plasticity. Plasticity of epithelial stem cells in tissue regeneration. Science. 344(6189):1242281.

Chai Y, Klauser DK, Denny PA, Denny PC. 1993. Proliferative and structural differences between male and female mouse submandibular glands. Anat Rec. 235(2):303–311.

Denny PC, Ball WD, Redman RS. 1997. Salivary glands: a paradigm for diversity of gland development. Crit Rev Oral Biol Med. 8(1):51–75.

Denny PC, Chai Y, Klauser DK, Denny PA. 1993. Parenchymal cell proliferation and mechanisms for maintenance of granular duct and acinar cell populations in adult male mouse submandibular gland. Anat Rec. 235(3):475–485.

Denny PC, Chai Y, Pimprapaiporn W, Denny PA. 1990. Three-dimensional reconstruction of adult female mouse submandibular gland secretory structures. Anat Rec. 226(4):489–500.

Denny PC, Denny PA, Chai Y, Klauser DK. 1993. DNA synthesis and development strategies with possible consequences on sexual dimorphism in adult mouse submandibular glands. Crit Rev Oral Biol Med. 4(3–4):511–516.

Emmelin N, Garrett JR, Ohlin P. 1968. Neural control of salivary myoepithelial cells. J Physiol. 196(2):381–396.

Gresik EW. 1994. The granular convoluted tubule (gct) cell of rodent submandibular glands. Microsc Res Tech. 27(1):1–24.

Hogan BL, Barkauskas CE, Chapman HA, Epstein JA, Jain R, Hsia CC, Niklason L, Calle E, Le A, Randell SH, et al. 2014. Repair and regeneration of the respiratory system: complexity, plasticity, and mechanisms of lung stem cell function. Cell Stem Cell. 15(2):123–138.

Ihrler S, Blasenbreu-Vogt S, Sendelhofert A, Rössle M, Harrison J, Löhrs U. 2004. Regeneration in chronic sialadenitis: an analysis of proliferation and apoptosis based on double immunohistochemical labelling. Virchows Arch. 444(4):356–361.

Ihrler S, Zietz C, Sendelhofert A, Lang S, Blasenbreu-Vogt S, Löhrs U. 2002. A morphogenetic concept of salivary duct regeneration and metaplasia. Virchows Arch. 440(5):519–526.

Kwak M, Ghazizadeh S. 2015. Analysis of histone h2bgfp retention in mouse submandibular gland reveals actively dividing stem cell populations. Stem Cells Dev. 24(5):565–574.

Lajtha LG. 1979. Stem cell concepts. Differentiation. 14(1–2):23–34.

Mao X, Fujiwara Y, Chapdelaine A, Yang H, Orkin SH. 2001. Activation of egfp expression by cre-mediated excision in a new rosa26 reporter mouse strain. Blood. 97(1):324–326.

Melnick M, Jaskoll T. 2000. Mouse submandibular gland morphogenesis: a paradigm for embryonic signal processing. Crit Rev Oral Biol Med. 11(2):199–215.

Nelson DA, Manhardt C, Kamath V, Sui Y, Santamaria-Pang A, Can A, Bello M, Corwin A, Dinn SR, Lazare M, et al. 2013. Quantitative single cell analysis of cell population dynamics during submandibular salivary gland development and differentiation. Biol Open. 2(5):439–447.

Ogawa Y, Toyosawa S, Ishida T, Ijuhin N. 2000. Keratin 14 immunoreactive cells in pleomorphic adenomas and adenoid cystic carcinomas of salivary glands. Virchows Arch. 437(1):58–68.

Pringle S, Van Os R, Coppes RP. 2013. Concise review: adult salivary gland stem cells and a potential therapy for xerostomia. Stem Cells. 31(4):613–619.

Redman RS. 2008. On approaches to the functional restoration of salivary glands damaged by radiation therapy for head and neck cancer, with a review of related aspects of salivary gland morphology and development. Biotech Histochem. 83(3–4):103–130.

Redman RS, Sreebny LM. 1970. The prenatal phase of the morphosis of the rat parotid gland. Anat Rec. 168(2):127–137.

Rios AC, Fu NY, Lindeman GJ, Visvader JE. 2014. In situ identification of bipotent stem cells in the mammary gland. Nature. 506(7488):322–327.

Schwartz-Arad D, Arber L, Arber N, Zajicek G, Michaeli Y. 1988. The rat parotid gland: a renewing cell population. J Anat. 161:143–151.

Tucker AS. 2007. Salivary gland development. Semin Cell Dev Biol. 18(2):237–244.

Waghmare SK, Bansal R, Lee J, Zhang YV, McDermitt DJ, Tumbar T. 2008. Quantitative proliferation dynamics and random chromosome segregation of hair follicle stem cells. Embo J. 27(9):1309–1320.

Zajicek G, Schwartz-Arad D, Arber N, Michaeli Y. 1989. The streaming of the submandibular gland. II: Parenchyma and stroma advance at the same velocity. Cell Tissue Kinet. 22(5):343–348.

Zajicek G, Yagil C, Michaeli Y. 1985. The streaming submandibular gland. Anat Rec. 213(2):150–158.